Aberystwyth University

Stability of the Surface Electron Accumulation Layers on the Nonpolar (1010) and (1120) Faces of ZnO

Heinhold, Robert; Cooil, Simon P.; Evans, D. Andrew; Allen, Martin W.

Stability of the surface electron accumulation on the non-polar $(10\bar{1}0)$ and $(11\bar{2}0)$ faces of ZnO

R. Heinhold,[1] S.P. Cooil,[2] D.A. Evans,[2] and M. W. Allen[1]

[1]*The MacDiarmid Institute for Advanced Materials and Nanotechnology, University of Canterbury, Christchurch 8043, New Zealand.*

[2]*Department of Mathematics and Physics, Aberystwyth University, Aberystwyth SY23 3BZ, United Kingdom.*

ABSTRACT

The stability of the ubiquitous hydroxyl termination and downward band bending on the m-plane $(10\bar{1}0)$ and a-plane $(11\bar{2}0)$ faces of ZnO single crystals was investigated using synchrotron and real-time x-ray photoelectron spectroscopy. On these non-polar surfaces, a strong correlation was found between the surface band bending and surface OH coverage, both of which could be modified via heat treatment in ultra high vacuum (UHV). On the m-plane $(10\bar{1}0)$ face, a threshold temperature of ~400 $^{\circ}$C was observed, after which there was a sudden increase in OH desorption and upwards movement of the near-surface bands, leading to a metallic-to-semiconductor transition in the electronic nature of the surface, and a change from surface electron accumulation to depletion. This loss of surface metallicity is associated with the disruption of a stable monolayer of chemisorbed hydroxyl groups that form a closed hydrogen-bonded network, across the rows of Zn–O dimers, on the m-plane $(10\bar{1}0)$ face. The downward band bending and surface electron accumulation layers on both the m-plane $(10\bar{1}0)$ and a-plane $(11\bar{2}0)$ faces could be modified and eventually removed by simple UHV heat treatment, with important implications for the processing and electrical performance of ZnO nanostructures and catalytic ZnO nanopowders, which usually contain a high proportion of these non-polar surfaces.

I. INTRODUCTION

ZnO is a transparent, wide band gap semiconductor whose electronically active surfaces are employed in a variety of applications, including high frequency surface acoustic wave generation, heterogeneous catalysis, and gas/bio-sensing.[1-3] The common low-index surfaces of ZnO are the Zn-polar (0001) and O-polar ($000\bar{1}$) faces that are bulk-terminated by entire outer planes of Zn and O atoms respectively, and the non-polar m-plane ($10\bar{1}0$) and a-plane ($11\bar{2}0$) faces that are mixed-terminated, consisting of Zn–O dimers in different configurations along the surface, as shown in Figs. 1(a)–(b).

ZnO surfaces are characterized by an unusual metallic nature due to the presence of a 2-dimensional electron accumulation layer, created by the downward bending of the near-surface bands in response to donor-like surface states.[4-9] At the same time, x-ray photoemission spectroscopy (XPS) studies have shown that, in most conditions, the polar and non-polar surfaces of ZnO are terminated by hydroxyl groups.[10-12]

However, the stability of the hydroxyl termination and its association with the metallic nature of the surface appears to be different for different ZnO surfaces. The hydroxyl termination on the O-polar ($000\bar{1}$) face is formed by hydrogen attached to the outer O atoms. The extent of the H coverage can be reversibly modified by heat treatment in ultra high vacuum (UHV) conditions, with a metallic to semiconductor-like transition in the electronic nature of the surface as the H coverage is reduced.[5,13] On the Zn-polar (0001) face, the hydroxyl termination is formed by OH groups on top of the outer Zn atoms.[14] The electron accumulation layer on this face has a significantly higher thermal stability, and consequently semiconductor-like (i.e. electron depleted) Zn-polar (0001) surfaces are more difficult to prepare.[13]

The nature of the hydroxyl termination on the non-polar faces of ZnO is more complex, with a mixed adlayer of H, OH and H_2O species likely to be involved.[15-17] Furthermore, the possibility of hydrogen bonding between these various species provides an additional variable in the stability and configuration of the surface hydroxyl coverage.[16-21] Hydroxylation of non-polar ZnO surfaces occurs across the trenches that separate the rows of Zn–O surface dimers, with H_2O molecules initially binding to the coordinatively unsaturated Zn surface atoms via a lone pair orbital.

In the case of the m-plane ($10\bar{1}0$) face, the Zn–O dimers run perpendicular to the direction of the surface trenches and consequently the trench edges consist of continuous rows of Zn and O surface atoms

[see Fig. 1(a)]. This provides a well-ordered template that promotes hydrogen bonding in a 2-dimensional 'key-lock' network between chemisorbed H_2O molecules and adjacent O surface atoms, and also between neighboring H_2O molecules.[16,17] A series of first principles and surface microscopy studies[16-21] have predicted that, at monolayer coverages, this hydrogen bonding network promotes the partial dissociation of half the H_2O molecules, forming a H_2O:OH:H network with a regular (2×1) periodicity [Fig. 1(c)].

The peculiar nature of the surface hydroxyls on the m-plane ($10\bar{1}0$) face of ZnO was first recognized by Nagao and co-workers,[22-24] who performed a series of investigations into the chemisorption and physisorption of water on prism-shaped ZnO powders, containing a high proportion of well-developed m-plane surfaces. A pronounced increase in the differential heat of chemisorption of water with increasing hydroxyl coverage was observed, reaching a maximum when the coverage approached a complete monolayer.[24] This unusual behavior was explained by the formation of a closed homogeneous monolayer network of surface hydroxyls, containing up to three hydrogen bonds per chemisorbed water molecule. It was further proposed that this strongly hydrogen-bonded network weakens the interaction with further water molecules and was responsible for the unusual (two-dimensional condensation) anomaly in the physisorption of water on ZnO.[22,23]

The a-plane ($11\bar{2}0$) face of ZnO is more stepped, with the Zn–O dimers running parallel to the direction of wider and deeper trenches, whose edges consist of rows of alternating Zn and O surface atoms [Fig. 1(b)]. Consequently, the adsorbed H_2O configuration is less symmetric, which is thought to lead to reduced intra-molecular H_2O hydrogen bonding. Cooke et al.[25] proposed that this reduced intra-molecular hydrogen bonding energetically favors full rather than partial H_2O dissociation on the a-plane ($11\bar{2}0$) face [see Fig. 1(d)]. Other authors[26,27] have noted that the energy difference between dissociative and associative adsorption is rather low and that the amount of dissociation may increase at higher (> 1 ML) coverages.[28,29] However, very few experimental studies have been carried out on ZnO ($11\bar{2}0$) surfaces and much less in known about the nature of their hydroxylation.

An understanding of the relationship between the chemical termination and electronic nature of the non-polar m-plane ($10\bar{1}0$) and a-plane ZnO ($11\bar{2}0$) surfaces is particularly important as they comprise a significant fraction of the exposed surface area of a wide variety of ZnO nanostructures, and also the micro- and nanocrystalline powders used in heterogeneous catalysis, antifungal coatings and biological UV filters.

In this work, we use a combination of variable photon energy synchrotron and real-time *in situ* XPS to study the stability of the hydroxyl termination and the surface electron accumulation on the non-polar faces of ZnO. XPS is a valuable tool for investigating the nature of semiconductor surfaces, allowing both the surface chemistry and electronic band bending to be simultaneously determined.

II. EXPERIMENTAL

Investigations into the fundamental properties of different ZnO surfaces are facilitated by the availability of freestanding, bulk single crystals that can be cleaved and chemomechanically polished to provide a variety of pristine, low defect surfaces. In this study, we have used 0.5 mm thick hydrothermally grown m-plane ($10\bar{1}0$) and a-plane ($11\bar{2}0$) single crystal wafers from Tokyo Denpa Co. (Japan),[30] cut to an offset of less than 0.5°. The resistivity, carrier concentration and electron mobility of the wafers used were typically 7 Ωcm, 5 $\times$ 10^{15} cm^{-3}, and 180 cm^{2}V^{-1}s^{-1}, respectively. The as-received wafers were ultrasonically cleaned using acetone, methanol, and isopropyl alcohol, and then dried with N$_2$ gas. Surface sensitive XPS analysis was then performed at the soft x-ray beamline of the Australian Synchrotron on as-loaded wafers and then after ~15 minute UHV heat treatments at 100 °C increments up to 700 °C. The XPS measurements were carried out at room temperature (RT) at a base pressure of < 2 $\times$ 10^{-10} mbar, with the heat treatments performed in a separate UHV preparation chamber. Each wafer was electrically grounded to the spectrometer via a tantalum foil sample holder and platinum paste, to avoid sample charging and to enable the zero of the binding energy (BE) scale to be directly reference to the Fermi level of each sample. The BE scale was in turn calibrated using the Au 4f core level doublet and Fermi edge of a sputter-cleaned Au reference foil.

The hydroxyl coverage was quantified using the relative component areas of O 1s core level spectra, acquired using hv = 680 eV x-rays and fitted using pseudo-Voigt functions on a Shirley background, with the full width at half maximum and the energetic separation of the component peaks constrained. The monolayer coverage was calculated from the OH peak area (A_{OH}) using a Lambert-Beer adsorption law approximation,[31,32] i.e. A_{OH}/A_{O1s} = [1 − exp(-d/l)], where A_{O1s} is the total O 1s signal, d the hydroxyl layer thickness, and l the photoelectron inelastic mean free path. For a photon energy of 680 eV, the kinetic

energy of photoelectrons emitted from the O 1s core level is ~150 eV, which corresponds to an inelastic mean free path l of ~6.2 Å, using the TPP-2M formula.[33] Following the approach employed by Önsten et al.,[32] the thickness of one monolayer of hydroxyls on the ZnO surface was taken to be 2.3 Å, which is the approximate distance between the O atoms in the surface OH termination (on either the Zn-polar, O-polar and non-polar faces) and the next nearest plane of lattice O atoms.

At the same time, the near surface band bending was determined from valence band (VB) spectra, collected using hv = 150 eV photons to maintain approximately the same photoelectron kinetic energy (~150 eV) as for the O 1s spectra. Using the approach of Chambers et al.,[34,35] the energetic separation ζ between the valence band maximum (E_V) and the Fermi level (E_F) in the near-surface region was extracted from a linear fit of the low BE edge of the VB spectrum to a line fitted to the instrument background. This was then used to determine the near-surface band bending V_{bb} using $V_{bb} = E_g - \zeta - \xi$, where $\xi = (kT/q)ln(N_C/n)$ is the energy difference between E_F and the conduction band minimum (E_C) in the bulk of the sample (n is the bulk carrier concentration and N_C is the conduction band effective density of states = 2.94×10^{18} cm^{-3} for ZnO). Negative values of V_{bb} indicate downward surface band bending and electron accumulation, while positive values of V_{bb} correspond to upward band bending and electron depletion.

III. RESULTS

Figure 2 shows the (hv = 680 eV) O 1s core level spectra, (hv = 150 eV) VB spectra, and extracted energy band diagrams for the as-loaded m-plane ($10\overline{1}0$) and a-plane ($11\overline{2}0$) surfaces. As the base pressure in the UHV system at the Australian Synchrotron was better than 2×10^{-10} mbar, most of the weakly physisorbed water on the surface of these as-loaded samples is likely to immediately evaporate,[22,28] leaving close to monolayer coverages of either associatively or dissociatively chemisorbed H_2O. The as-loaded O 1s spectra are shown in Figs. 2(a)–2(b) and are dominated by two components - a low BE component due to bulk O (i.e. O atoms tetrahedrally coordinated to four Zn atoms) and a higher BE component attributed to O atoms in surface-terminating OH groups. A third much smaller component near the high BE tail of the O 1s spectra is associated with molecular H_2O.[13] The relative peak area of the OH component provides a direct indication of the OH coverage on each face. The relatively small peak area of the H_2O component on

the m-plane ($10\overline{1}0$) face is rather surprising given the large amount of literature proposing a 1:1 H_2O:OH equilibrium as the lowest surface energy configuration for chemisorbed H_2O.[16-21] However, the extensive hydrogen bonding experienced by chemisorbed H_2O molecules on the m-plane ($10\overline{1}0$) surface may result in a similar binding energy for O atoms in both OH and H_2O species in the first monolayer. Alternatively the incident x-rays used in XPS may provide sufficient energy to promote full H_2O dissociation within the first monolayer. In either case, the H_2O component is more likely to be due to 'diffuse' H_2O molecules physisorbed on top of the closed hydrogen bonded network of the first monolayer.

The corresponding VB spectra, shown in Figs. 2(c)–2(d), contain two main features – a low BE peak I due to O $2p$ derived states and a higher BE peak II that has a hybridized O $2p$, Zn $4s$, and Zn $3d$ character.[6,12] The linear fit to the low BE edge of the VB emission and the extracted values of the parameter ζ are also shown. For each face, the value of ζ (along with ξ and E_g) was used to construct energy band diagrams, as shown in Figs. 2(e)–2(f). These indicate significant downward band bending on both non-polar faces, and in each case the Fermi level lies in the conduction band, consistent with surface electron accumulation. Interestingly, the downward band bending is significantly stronger on the as-loaded a-plane ($11\overline{2}0$) face, which may be related to the significantly larger OH component in the corresponding O $1s$ spectra.

Figure 3 shows the evolution of the O $1s$ and VB spectra on the m-plane ($10\overline{1}0$) and a-plane ($11\overline{2}0$) faces after each ~15 min heat treatment up to 600 °C. Both faces show a significant reduction in OH coverage with temperature [Figs. 3(a)–(b)] combined with a consistent negative shift in the energetic position of both the O $1s$ and VB spectra [Figs. 3(c)–(d)] indicating a significant upwards movement of the near-surface bands.

The O $1s$ spectra in Figs. 3(a)–(b) were used to construct plots of the relative peak areas of the OH and H_2O components (A_{OH} and A_{H2O} respectively) versus heat treatment temperature for the m-plane ($10\overline{1}0$) and a-plane ($11\overline{2}0$) faces. These are shown in Fig. 4(a) together with equivalent data from an identical experiment performed on the Zn-polar (0001) and O-polar ($000\overline{1}$) faces of a double-sided polished hydrothermal ZnO single crystal wafer, also from Tokyo Denpa Co.[13] The right hand scale shows the OH coverage expressed in monolayers, using the approximations outlined in Sec. II. There is a significant

difference in the stability of the OH coverage on the non-polar faces of ZnO compared to the polar faces, with a much larger thermal reduction in OH coverage observed for the non-polar faces, particularly the m-plane ($10\overline{1}0$) face which is almost hydroxyl free after 600 – 700 $^{\circ}$C UHV heat treatment.

Similarly, the VB spectra in Figs. 3(c)–(d) were used to construct plots of surface band bending V_{bb} versus heat treatment temperature for the m-plane ($10\overline{1}0$) and a-plane ($11\overline{2}0$) faces, that are shown in Fig. 4(b), alongside equivalent data for the polar ZnO faces.[13] A comparison of Figs. 4(a) and 4(b) shows an inverse correlation between the OH coverage and the surface band bending (V_{bb}) for both the m-plane and a-plane faces. As such, the behavior of the non-polar faces is similar to that observed for the O-polar ($000\overline{1}$) face, in that the downward band bending (and the surface electron accumulation) can be removed by simple UHV heat treatment. This is in direct contrast to the Zn-polar (0001) face, whose OH termination and downward band bending is largely unaffected by the same heat treatment process.

Figures 4(a) and 4(b) also reveal interesting differences in the behavior of the two non-polar faces: The surface hydroxyl coverage and downward band bending both appear to be significantly larger on the a-plane ($11\overline{2}0$) face. In the case of the m-plane ($10\overline{1}0$) face, there is a distinct plateau in the thermal desorption of the OH coverage. After an initial reduction after 170 $^{\circ}$C, the OH coverage is almost constant for heat treatments between 170 – 400 $^{\circ}$C. This is followed by a sudden step-like decrease in OH coverage between the 400 $^{\circ}$C and 500 $^{\circ}$C heat treatments, that is accompanied by a large positive increase (i.e. upward shift) in the surface band bending V_{bb}. For the a-plane ($11\overline{2}0$) face, the thermal desorption of the surface OH coverage and the corresponding changes in V_{bb} are rather more linear with temperature, although there is also a suggestion of a similar step-like change between 400 – 500 $^{\circ}$C.

Interestingly, a sudden increase in the 'diffuse' H_2O component was observed on both non-polar faces after the 400 $^{\circ}$C heat treatment, that was not seen on either of the polar faces. For the m-plane ($10\overline{1}0$) face, this may correspond to the thermal disruption of the closed hydrogen bonding network of the first H_2O:OH:H monolayer and the formation of more weakly bonded H_2O molecules, that are then able to more readily desorb from the surface. This could explain the sudden decrease in OH coverage between the 400 $^{\circ}$C and 500 $^{\circ}$C heat treatments, which can occur via condensation-dehydration once the energy barrier associated with breaking the strongly hydrogen-bonded monolayer network is overcome.

The non-linear temperature stability of the band bending on the m-plane ($10\bar{1}0$) face was further investigated via real-time XPS measurements, taken during the UHV heating of a similar hydrothermal m-plane ($10\bar{1}0$) ZnO single crystal wafer, from RT to 650 ^{o}C over approximately 90 mins. These real-time measurements were carried out at the University of Aberystwyth, using Mg K$_\alpha$ (1253.6 eV) radiation and a Spec Phoibos 100 hemispherical electron analyzer coupled to a multichannel (768 channel) electron-counting array,[36,37] that enabled complete snapshot Zn $2p_{3/2}$ and O $1s$ core level spectra to be acquired at 1-sec intervals throughout the heating cycle. The wafer was electrically grounded to the spectrometer via a molybdenum sample holder, so that the Fermi-level could again be referenced to the zero of the BE scale. The BE position of the peak maximum of each snapshot Zn $2p_{3/2}$ spectrum, extracted from a fitted pseudo-Voight function, was used to monitor changes in surface band bending (V_{bb}) during the heating cycle. Negative shifts in Zn $2p_{3/2}$ BE position correspond to a positive shift in V_{bb} and an upwards movement of the near surface bands (i.e. either a reduction in downward band bending or an increase in upward band bending).

Figure 5 shows the real-time BE shift of the Zn $2p_{3/2}$ peak versus temperature for the m-plane ($10\bar{1}0$) face. The most obvious feature is a sudden increase in negative BE shift at ~400 ^{o}C, indicating a significant increase in the rate of upward movement of the near surface bands. This is consistent with the results of the synchrotron experiment in which a step-like increase in both OH desorption and V_{bb} was observed between the 400 and 500 ^{o}C heat treatments. There are other similarities in that Fig. 5 also shows evidence of a small negative BE shift up to ~200 ^{o}C, followed by a plateau region between 200 – 400 ^{o}C.

IV. DISCUSSION

The stability of the hydroxyl termination and downward band bending on the non-polar m-plane ($10\bar{1}0$) and a-plane ($11\bar{2}0$) faces of ZnO is significantly different compared to their polar counterparts, i.e. the O-polar ($000\bar{1}$) and Zn-polar (0001) faces.

Firstly, thermal desorption of the OH termination is much stronger on the non-polar ZnO faces [see

Fig. 4(a)]. On the m-plane ($10\bar{1}0$) face, an almost 'bare' hydroxyl-free surface was realized after 600 – 700 ^{o}C heating in UHV, in contrast to the O-polar ($000\bar{1}$) face for which a thermal desorption limit of ~0.5 ML OH coverage appears to exist, and the Zn-polar (0001) face whose OH termination is much more resilient to heat treatment.[13] Significantly, the non-polar faces of ZnO are free of out-of-plane electric fields and are electrostatically stable in their unreconstructed bulk-terminated form.[16,38] Consequently, polar adsorbates, such as H and OH, are not required to play any stabilizing role on non-polar ZnO surfaces, and this may contribute to the lower thermal stability of the OH termination on these faces. This is not the case for the O-polar and Zn-polar faces, for which first-principles studies predict that an OH termination of ~0.5 ML is highly effective in stabilizing their intrinsic electrostatic instability.[39-41]

Secondly, the surface OH coverage decreases steadily with heat-treatment temperature on the polar ZnO faces, while on the m-plane ($10\bar{1}0$) face the OH desorption is 'step-like' in nature, with an almost constant coverage between 170 – 400 ^{o}C followed by a sudden decrease between 400 – 500 ^{o}C [see Fig. 4(a)]. Nagao et al.[24] reported a similar step-like decrease, between 200 ^{o}C and 400 ^{o}C, in the concentration of surface hydroxyls on ZnO powders that contained a high proportion of m-plane ($10\bar{1}0$) surface area. This was accompanied by a sharp increase in the heat of immersion in water for samples heat-treated over the temperature range, while for heat treatments above 400 ^{o}C the heat of immersion was nearly constant. This behavior was associated with the formation of a closed monolayer network of strongly hydrogen-bonded surface hydroxyls.[24] It is therefore likely that that the 'plateau region' in Fig. 4(a) between 170 – 400 ^{o}C, where the OH coverage on the m-plane face remains almost constant, corresponds to this predicted closed monolayer network, probably in the form of a half dissociated 1:1:1 H_2O:OH:H structure.[16-21] The estimated OH coverage for this 'plateau region' in Fig. 4(a) is ~1.2 ML (using the assumptions described in Sec. II) which is remarkably close to a single monolayer, given the approximations involved in the calculation of surface monolayers.

In other work, Morishige et al.[42] reported two distinct peaks in the thermal desorption spectra (TDS) of chemisorbed water on hydroxylated ZnO powders at 220 ^{o}C and 270 ^{o}C, with the latter being correlated with a reduction of a broad peak at 3540 cm^{-1} in infrared adsorption spectra that was attributed to surface hydroxyls. Martin et al.[43] also observed two well-defined peaks in the TDS of H_2O from ZnO powders at approximately 200 ^{o}C and 400 ^{o}C, with the 400 ^{o}C desorption peak being significantly stronger. They also

reported a correlation between the rate of H_2O desorption and anomalous peaks in the complex permittivity of the powdered samples, indicating accompanying changes in the electrical nature of their samples.

In this work, the correlation between the hydroxyl coverage and the electronic nature of the ZnO surface can be clearly seen in Fig. 6, which shows the surface band bending V_{bb} versus the OH coverage (in monolayers) for each face, constructed from the synchrotron data in Figs. 4(a)–(b). It is important to keep in mind that the OH coverage on the O-polar, Zn-polar, and non-polar faces will involve different adsorbed species, i.e. H, OH, and H_2O:OH:H, respectively. Two monolayer scales are shown in Fig. 6, the lower scale uses the Lambert-Beer approximation as described in Sec. II [and previously used in Fig. 4(a)], while the upper scale is based on the physical argument (explained earlier in this section) that the 'plateau region' in the thermal OH desorption from the m-plane ($10\bar{1}0$) face corresponds to a closed hydroxyl monolayer.

Figure 6 shows a similar inverse correlation between OH coverage and V_{bb} for the m-plane ($10\bar{1}0$) and a-plane ($11\bar{2}0$) faces. On both these non-polar faces, the downward band bending (and by association the surface electron accumulation) could be reduced and eventually removed by decreasing the OH coverage, via simple UHV heating. In the case of the m-plane ($10\bar{1}0$) face, the near-surface bands could be bent upwards (corresponding to surface electron depletion) as the OH coverage was further reduced, reaching an upwards band bending of + 0.3 eV, after 600 ^{o}C UHV heating. On the a-plane ($11\bar{2}0$) face, flat band conditions were achieved following the same 600 ^{o}C heat-treatment. The stronger downward band bending on the a-plane face can also be seen at sub-monolayer OH coverages in Fig. 6, where V_{bb} is consistently lower (by ~0.1 meV) for the same OH coverage.

Figure 6 also shows that the response of the m-plane ($10\bar{1}0$) face to surface hydroxyl removal is similar to the O-polar ($000\bar{1}$) face, in that the electronic nature of the surface can be switched from electron accumulation (downward band bending) to electron depletion (upward band bending) by reducing the OH coverage. However, there are also important differences, in that the rate of increase of V_{bb} with decreasing OH coverage is considerably larger for the O-polar face. The residual OH coverage on the O-polar face is also much larger, close to the theoretically predicted 0.5 ML limit,[39-41] while for the m-plane ($10\bar{1}0$) face almost 'bare' hydroxyl-free surfaces can be realized using just simple UHV heating. Furthermore, low energy electron diffraction (LEED) patterns measured throughout the UHV heating cycle

(inset of Fig. 5) were unchanged, indicating a (1×1) surface structure at all temperatures, which suggests that hydroxyl removal does not induce any reconstruction of the m-plane ($10\bar{1}0$) face.

Remarkably, the transition from downward to upward band bending (corresponding to flat-band conditions where $V_{bb} = 0$) occurs at the same OH coverage for both the m-plane ($10\bar{1}0$) and O-polar ($000\bar{1}$) faces (see Fig. 6). This is ~0.9 ML using the Lambert Beer approximation or ~0.75 ML using the 'closed monolayer' argument. Table I shows the OH coverage (using the latter approach) and the corresponding surface band bending (V_{bb}) for as-loaded samples, flat-band conditions, and after 600 ^{o}C UHV heating, for the common faces of ZnO. It is perhaps surprising that the as-loaded OH (i.e. UHV) coverages for the m-plane ($10\bar{1}0$) and a-plane ($11\bar{2}0$) faces are greater than 1 ML, given the reported weak physisorption anomaly for H_2O on the m-plane face.[22] However, Raymand et al.[28,29] considered water adsorption for coverages beyond a single monolayer on ZnO m-plane ($10\bar{1}0$) surfaces and predicted that a second layer of water molecules could lead to significantly increased hydroxylation of the first monolayer, with surface OH groups forming a new hydrogen bond network with H_2O molecules in the second layer.

V. SUMMARY AND CONCLUSIONS

Under most conditions, bare ZnO surfaces chemisorb water molecules to a form a surface hydroxyl termination on top of which further water molecules may be more weakly physisorbed. Hydroxylation of the ZnO surface dramatically changes its electronic nature, providing a source of shallow donors that bend the near-surface bands downward, creating unusual 2-dimensional electron accumulation layers. However, the nature and stability of the OH termination, and the accompanying surface metallicity, varies significantly with the crystallographic polarity of the surface.

On the non-polar m-plane ($10\bar{1}0$) and a-plane ($11\bar{2}0$) faces, the OH coverage and surface band bending were found to be strongly related, with flat band conditions realized when the OH coverage was reduced to ~0.75 ML and ~0.4 ML, respectively. As such, the behavior of these non-polar surfaces is similar to the O-polar ($000\bar{1}$) face, which shows an even steeper relationship, and in direct contrast to the Zn-polar (0001) face whose OH termination and surface electron accumulation are much more resilient to

thermal desorption.

The nature of the OH termination on the m-plane ($10\bar{1}0$) face of ZnO appears to be rather unique, in that it can be almost completely desorbed via a modest UHV heat treatment of only 600 – 700 ^{o}C, with most of this reduction occurring in a sudden 'step-like' decrease between 400 ^{o}C and 500 ^{o}C. This unusual behavior is associated with the thermal disruption of a closed hydrogen-bonded hydroxyl monolayer (most probably in the form of a theoretically predicted half-dissociated H_2O:OH:H network), after which the surface loses its metallicity and becomes semiconductor-like in nature, with upward band bending and near-surface electron depletion.

In general, the thermal stability of the hydroxyl termination on the non-polar faces of ZnO is significantly lower compared to their polar counterparts, due in part to their intrinsic electrostatic stability. Many first principles studies have also predicted a low energy difference between the associative and dissociated adsorption of H_2O on the m-plane ($10\bar{1}0$) face of ZnO. This suggests that recombination of dissociated H and OH species into molecular H_2O may be relatively straightforward, once sufficient energy is provided to break the strong hydrogen bonding network in the first H_2O:OH:H monolayer.

The ability to readily modify the chemical and electronic nature of the non-polar surfaces of ZnO, as demonstrated here using simple UHV heating, has important implications for the fabrication of device elements, such as ohmic contacts, Schottky junctions, and ZnO-based heterostructures. Furthermore, these findings also suggest that the electronic nature of ZnO nanostructures and catalytic nanocrystalline ZnO powders, that usually contain a high proportion of non-polar surface area, may also be modified via a similarly straightforward thermal process.

Cowie, L. Thomsen, and A. Tadich at the Australian Synchrotron, Victoria, Australia

REFERENCES

[1]C. Wöll, Progress in Surface Science **82**, 55 (2007).

[2]U. Özgür, D. Hofstetter, and H. Morkoç, Proc. IEEE **98**, 1255 (2010).

[3]S. K. Arya, S. Saha, J. E. Ramirez-Vick, V. Gupta, S. Bhansali, and S. P. Singh, Analytica Chimica Acta **737**, 1 (2012).

[4]O. Schmidt, A. Geis, P. Kiesel, C. G. Van de Walle, N. M. Johnson, A. Bakin, A. Waag, and G. H. Dohler, Superlatt. and Microstruct. **39**, 8 (2006).

[5]K. Ozawa and K. Mase, Phys. Rev. B **81**, 205322 (2010).

[6]M. W. Allen, C. H. Swartz, T. H. Myers, T. D. Veal, C. F. McConville, and S. M. Durbin, Phys. Rev. B **81**, (2010).

[7]L. F. J. Piper, A. R. H. Preston, A. Fedorov, S. W. Cho, A. DeMasi, and K. E. Smith, Phys. Rev. B **81**, 233305 (2010).

[8]K. Ozawa and K. Mase, Phys. Rev. B **83**, 125406 (2011).

[9]P. D. C. King and T. D. Veal, J. Phys.: Condens. Matter **23**, 334214 (2011).

[10]B. J. Coppa, C. C. Fulton, S. M. Kiesel, R. F. Davis, C. Pandarinath, J. E. Burnette, R. J. Nemanich, and D. J. Smith, J. Appl. Phys. **97**, 103517 (2005).

[11]M. Kunat, S. G. Girol, T. Becker, U. Burghaus, and C. Wöll, Phys. Rev. B **66**, 081402 (2002).

[12]M. W. Allen, D. Y. Zemlyanov, G. I. N. Waterhouse, J. B. Metson, T. D. Veal, C. F. McConville, and S. M. Durbin, Appl. Phys. Lett. **98**, 101906 (2011).

[13]R. Heinhold, G. T. Williams, S. P. Cooil, D. A. Evans, and M. W. Allen, Phys. Rev. B. **88**, 235315 (2013).

[14]C. M. Schlepütz, Y. Yang, N. S. Husseini, R. Heinhold, H.-S. Kim, M. W. Allen, S. M. Durbin, and R. Clarke, J. Phys.: Condens. Matter **24**, 095007 (2012).

[15]K. Morishige, S. Kittaka, T. Moriyasu, and T. Morimoto, J.C.S. Faraday Trans. I **76**, 728 (1980).

[16]B. Meyer, D. Marx, O. Dulub, U. Diebold, M. Kunat, D. Langenberg, and C. Woll, Angew. Chem., Int. Ed. **43**, 6642 (2004).

[17]O. Dulub, B. Meyer, and U. Diebold, Phys. Rev. Lett. **95**, 136101 (2005).

[18]Y. Yan and M. M. Al-Jassim, Phys. Rev. B **72**, 235406 (2005).

[19]B. Meyer, H. Rabaa, and D. Marx, Phys. Chem. Chem. Phys. **8**, 1513 (2006).

[20]Y. Wang, M. Muhler, and C. Woll, Phys. Chem. Chem. Phys. **8**, 1521 (2006).

[21]A. Calzolari and A. Catellani, J. Phys. Chem. C. **113**, 2896 (2006).

[22]M. Nagao, J. Phys. Chem. **75**, 3822 (1971).

[23]T. Morimoto and M. Nagao, J. Phys. Chem. **78**, 1116 (1974).

[24]M. Nagao, K. Yunoki, H. Muraishi, and T. Morimoto, J. Phys. Chem. **82**, 1032 (1978).

[25]D. J. Cooke, A. Marmier, and S. C. Parker, J. Phys. Chem. B **110**, 7985 (2006).

[26]S. groβe Holthaus, S. Köppen, T. Frauenheim, and L. Colombi Ciacchi, J. Chem. Theory Comput. **8**, 4517 (2012).

[27]M. Hellström, K. Jorner, M. Bryngelsson, S. E. Huber, J. Kullgren, T. Frauenheim, and P. Broqvist, J. Phys. Chem. C. **117**, 17004 (2013).

[28]D. Raymand, A. C.T. van Duin, W. A. Goddard, K. Hermansson, and D. Spangberg, J. Phys. Chem. C **115**, 8573 (2011).

[29]D. Raymand, T. Edvinsson, D. Spangberg, A. van Duin, and K. Hermansson, Proc. SPIE **7044**, 7044E (2008).

[30]K. Maeda, M. Sato, I. Niikura, and T. Fukuda, Semicond. Sci. Technol. **20**, S49 (2005).

[31]Y. Joseph, W. Ranke, and W. Weiss, J. Phys. Chem. B **104**, 3224 (2000)

[32]A. Önsten, D. Stoltz, P. Palmgren, K. Yu, T. Claesson, M. Göthelid, U. O. Karlsson, Surf. Sci. **608**, 31 (2013).

[33]S. Tanuma, C. J. Powell, and D. R. Penn, Surf. Interface Anal. **17**, 927 (1991).

[34]S. A. Chambers, T. Droubay, T. C. Kaspar, and M. Gutowski, J. Vac. Sci. Technol. B **22**, 2205 (2004).

[35]P. D. C. King, T. D. Veal, D. J. Payne, A. Bourlange, R. G. Egdell, and C. F. McConville, Phys. Rev. Lett. **101**, 116808 (2008).

[36]D. A. Evans, O. R. Roberts, A. R. Vearey-Roberts, D. P. Langstaff, D. J. Twitchen, and M. Schwitters,

Appl. Phys. Lett. **91**, 132114 (2007).

[37]D. A. Evans, O. R. Roberts, A. R. Vearey-Roberts, G. T. Williams, A. C. Brieva, and D. P. Langstaff, Appl. Phys. Lett. **102**, 021605 (2013).

[38]B. Meyer and M. Dominik, Phys. Rev. B **67**, 035403 (2003).

[39]G. Kresse, O. Dulub, and U. Diebold, Phys. Rev. B **68**, 245409 (2003).

[40]M. Valtiner, M. Todorova, G. Grundmeier, and J. Neugebauer, Phys. Rev. Lett. **103**, 065502 (2009).

[41]R. Wahl, J. V. Lauritsen, F. Besenbacher, and G. Kresse, Phys. Rev. B **87**, 085313 (2013).

[42]K. Morishige, S. Kittaka, T. Moriyasu, and T. Morimoto, J.C.S. Faraday Trans. I **76**, 728 (1980).

[43]L.P. Martin, D. Dadon, M. Rosen, D. Gershon, K.I. Rybakov, A. Birman, J.P. Calame, B. Levush, Y. Carmel, and R. Hutcheon, J. Appl. Phys. **83**, 432 (1998).

LIST OF FIGURES:

Fig. 1 (color online) Top view of the non-polar (a) m-plane ($10\bar{1}0$) and (b) a-plane ($11\bar{2}0$) faces of ZnO (dashed lines indicate the respective surface unit cells). The lowest energy $H_2O:OH:H$ configurations, predicted by first principles studies,[16-20] are illustrated in (c) and (d) respectively.

FIG. 2 (Color online) (a)-(b) O $1s$ core level XPS spectra, taken using $hv = 680$ eV synchrotron radiation, on the non-polar m-plane ($10\bar{1}0$) and a-plane ($11\bar{2}0$) faces of hydrothermal single crystal ZnO (Dots represent measured data points, full lines represent fitted pseudo-Voigt functions of the bulk oxygen, surface hydroxyl, and surface water components on a Shirley background); (c)-(d) valence band (VB) XPS spectra taken at $hv = 150$ eV showing the band bending parameter ζ obtained by extrapolating the low BE edge (red line) to the instrument background (blue line); (e)-(f) band bending schematic diagrams of the m-plane ($10\bar{1}0$) and a-plane ($11\bar{2}0$) faces.

FIG. 3 (Color online) (a)-(b) O $1s$ core level spectra ($hv = 680$ eV) and (c)-(d) valence band spectra ($hv = 150$ eV) taken on the m-plane ($10\bar{1}0$) and a-plane ($11\bar{2}0$) faces of hydrothermal single crystal ZnO, after successive 15 min UHV heat treatments.

FIG. 4 (Color online) (a) Relative peak area (left hand scale) of the OH and H_2O components of the respective O $1s$ spectra ($hv = 680$ eV) and calculated hydroxyl monolayer coverage (right hand scale) for the non-polar m-plane ($10\bar{1}0$) and a-plane ($11\bar{2}0$) faces, compared to the Zn-polar (0001) and O-polar ($000\bar{1}$) faces, of hydrothermal single crystal ZnO after successive 15 min UHV heat treatments; and (b) surface band bending (V_{bb}) versus temperature for same non-polar and polar ZnO faces extracted from valence band XPS spectra ($hv = 150$ eV), acquired at the same time.

FIG. 5 (Color online) Real-time binding energy shift in the position of the Zn $2p_{3/2}$ photoemission peak recorded from the m-plane ($10\bar{1}0$) face of hydrothermal single crystal ZnO versus temperature during

UHV heating. The inset shows the LEED pattern from the same m-plane face that was unchanged throughout the 'real-time' UHV heating cycle.

FIG. 6 (Color online) Surface band bending (V_{bb}) versus hydroxyl monolayer coverage on the non-polar m-plane ($10\overline{1}0$) and a-plane ($11\overline{2}0$) faces, and also for the Zn-polar (0001) and O-polar ($000\overline{1}$) faces, of hydrothermal single crystal ZnO extracted via synchrotron XPS following different UHV heat treatments. The horizontal dashed line represents flat near-surface bands. The lower monolayer scale (†) was calculated using a Lambert-Beer approximation, while the upper scale (‡) is based on the physical argument of a closed hydroxyl monolayer on the m-plane ($10\overline{1}0$) face between 200 and 400 $^{\circ}$C, as proposed by Nagao *et al*.[22-24]

TABLES:

Table I. OH monolayer coverage[‡] and surface band bending (V_{bb}) for as-loaded (UHV) conditions, flat band conditions, and after ~600 °C heat treatment, for the non-polar and polar faces of hydrothermal single crystal ZnO, extracted from Fig. 6 ([‡]using the upper monolayer scale).

Crystal face	As-loaded	Flat-band conditions	After ~600 °C
m-plane ($10\bar{1}0$)	1.5 ML	0.75 ML	0.2 ML
	- 0.3 eV	0 eV	+ 0.3 eV
a-plane ($11\bar{2}0$)	1.8 ML	0.4 ML	0.4 ML
	- 0.6 eV	0 eV	0 eV
O-polar ($000\bar{1}$)	1.0 ML	0.75 ML	0.5 ML
	- 0.3 eV	0 eV	+ 0.4 eV
Zn-polar (0001)	1.0 ML	n/a	0.8 ML
	- 0.6 eV		- 0.5 eV

Fig. 1 (color online) Top view of the non-polar (a) m-plane ($10\bar{1}0$) and (b) a-plane ($11\bar{2}0$) faces of ZnO (dashed lines indicate the respective surface unit cells). The lowest energy H$_2$O:OH:H configurations, predicted by first principles studies,[16-20] are illustrated in (c) and (d) respectively.
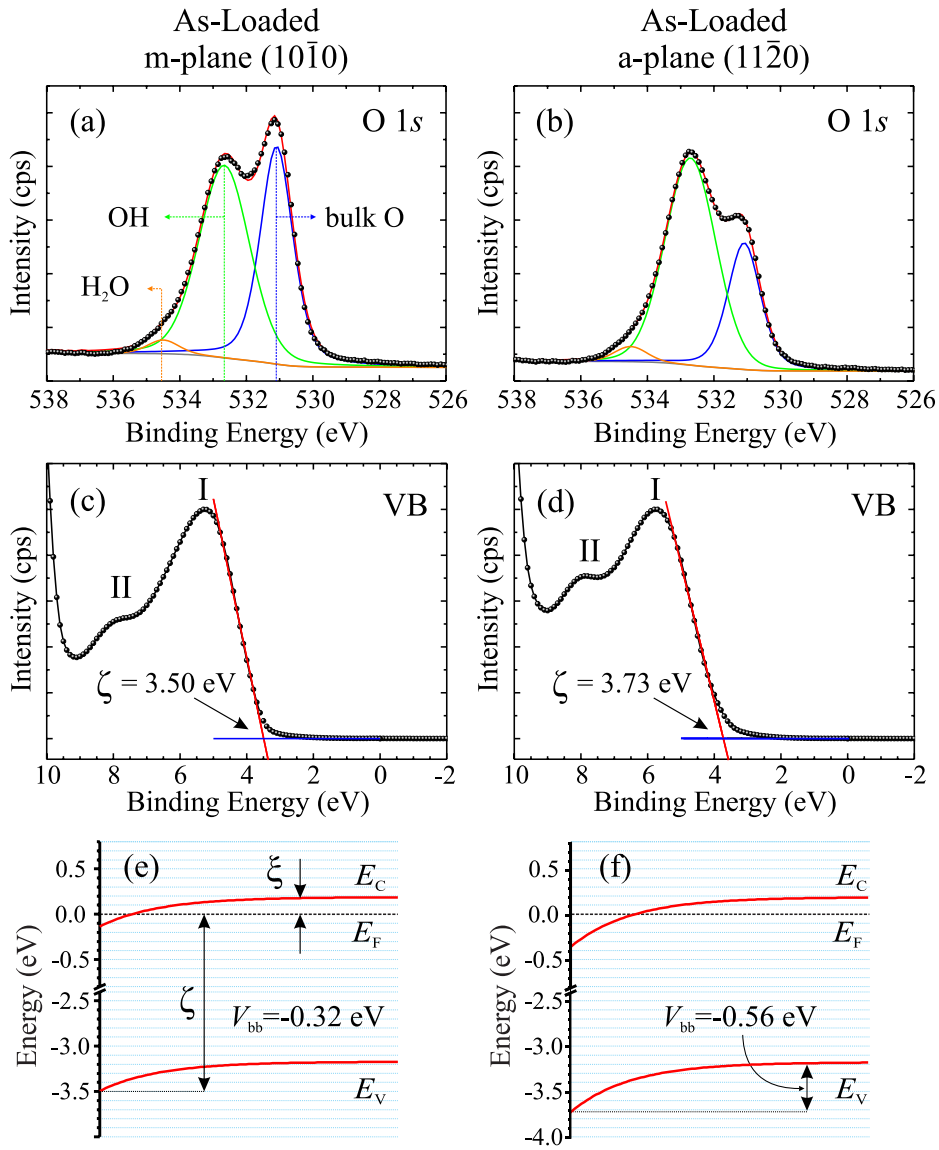
FIG. 2 (Color online) (a)-(b) O 1s core level XPS spectra, taken using hv = 680 eV synchrotron radiation, on the non-polar m-plane ($10\bar{1}0$) and a-plane ($11\bar{2}0$) faces of hydrothermal single crystal ZnO (Dots represent measured data points, full lines represent fitted pseudo-Voigt functions of the bulk oxygen, surface hydroxyl, and surface water components on a Shirley background); (c)-(d) valence band (VB) XPS spectra taken at hv = 150 eV showing the band bending parameter ζ obtained by extrapolating the low BE edge (red line) to the instrument background (blue line); (e)-(f) band bending schematic diagrams of the m-plane ($10\bar{1}0$) and a-plane ($11\bar{2}0$) faces.
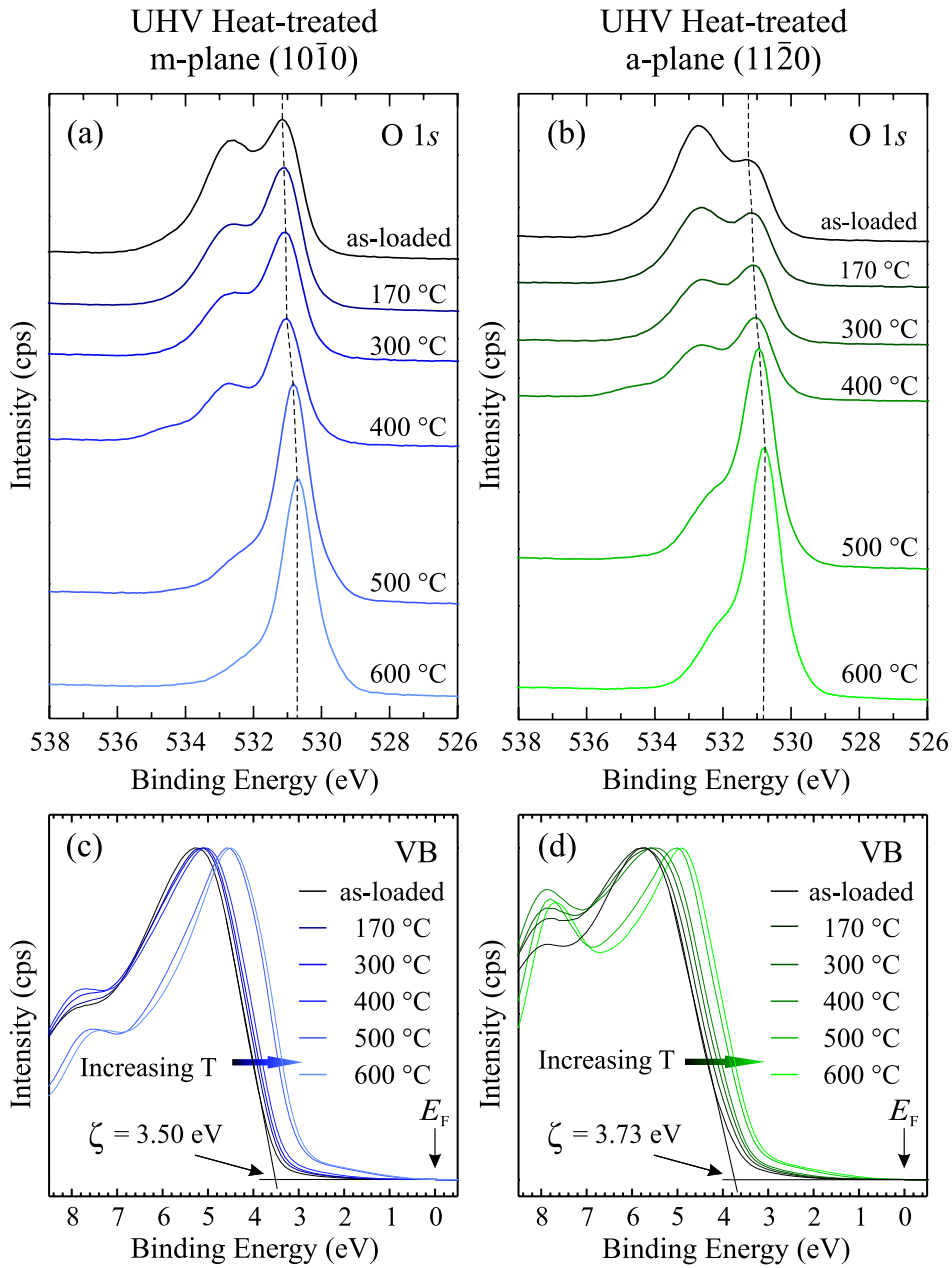
FIG. 3 (Color online) (a)-(b) O $1s$ core level spectra ($h\nu$ = 680 eV) and (c)-(d) valence band spectra ($h\nu$ = 150 eV) taken on the m-plane ($10\bar{1}0$) and a-plane ($11\bar{2}0$) faces of hydrothermal single crystal ZnO, after successive 15 min UHV heat treatments.
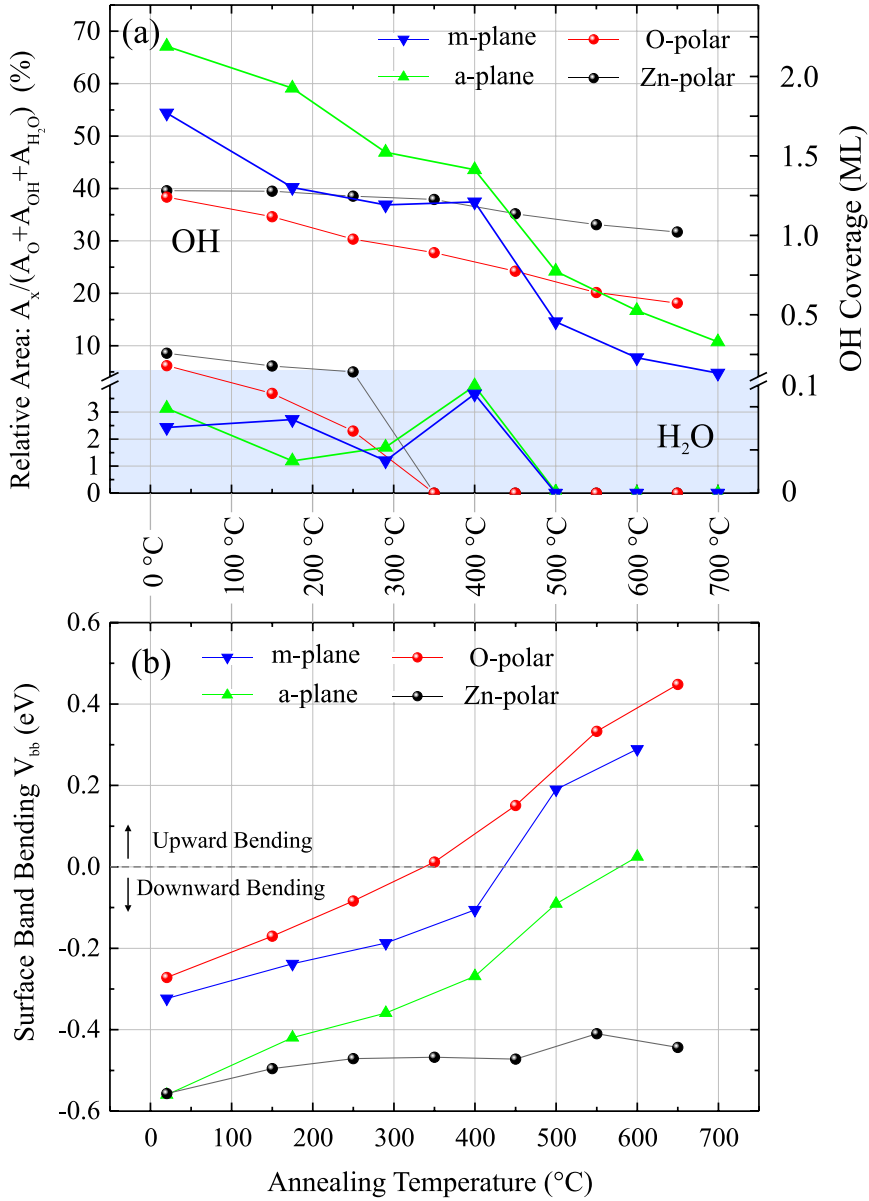
FIG. 4 (Color online) (a) Relative peak area (left hand scale) of the OH and H_2O components of the respective O $1s$ spectra (hv = 680 eV) and calculated hydroxyl monolayer coverage (right hand scale) for the non-polar m-plane ($10\bar{1}0$) and a-plane ($11\bar{2}0$) faces, compared to the Zn-polar (0001) and O-polar ($000\bar{1}$) faces, of hydrothermal single crystal ZnO after successive 15 min UHV heat treatments; and (b) surface band bending (V_{bb}) versus temperature for same non-polar and polar ZnO faces extracted from valence band XPS spectra (hv = 150 eV), acquired at the same time.
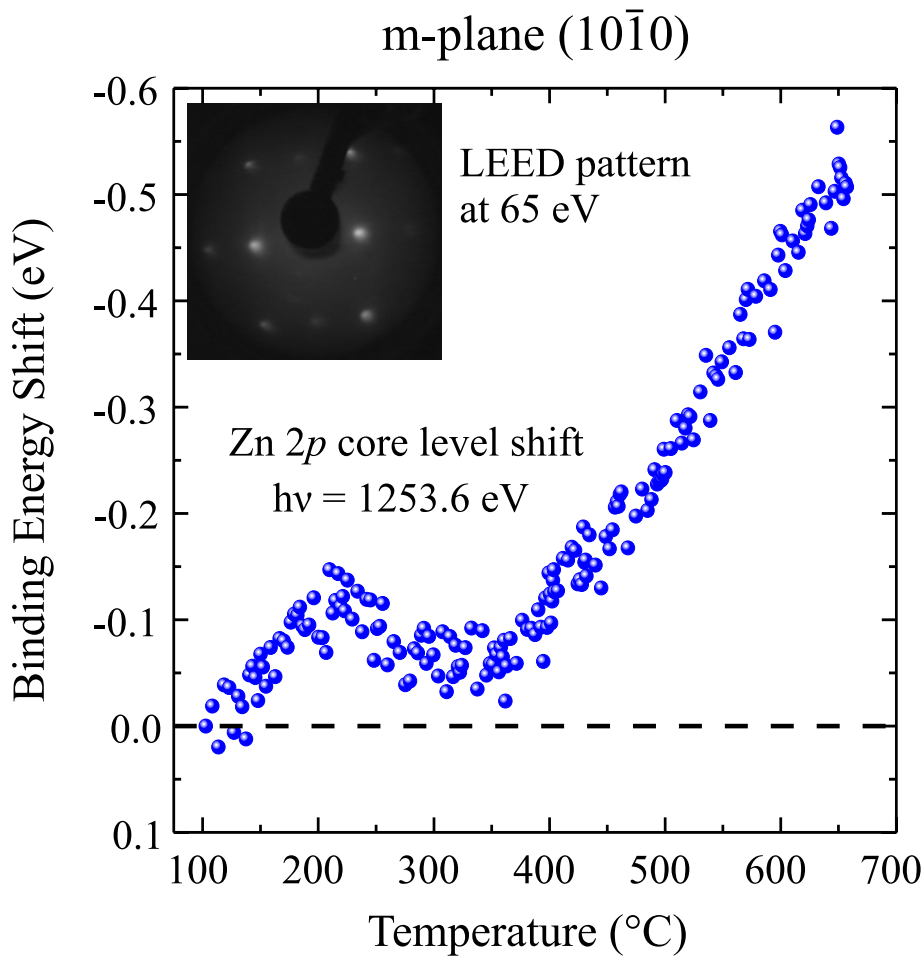
FIG. 5 (Color online) Real-time binding energy shift in the position of the Zn $2p_{3/2}$ photoemission peak recorded from the m-plane ($10\bar{1}0$) face of hydrothermal single crystal ZnO versus temperature during UHV heating. The inset shows the LEED pattern from the same m-plane face that was unchanged throughout the 'real-time' UHV heating cycle.
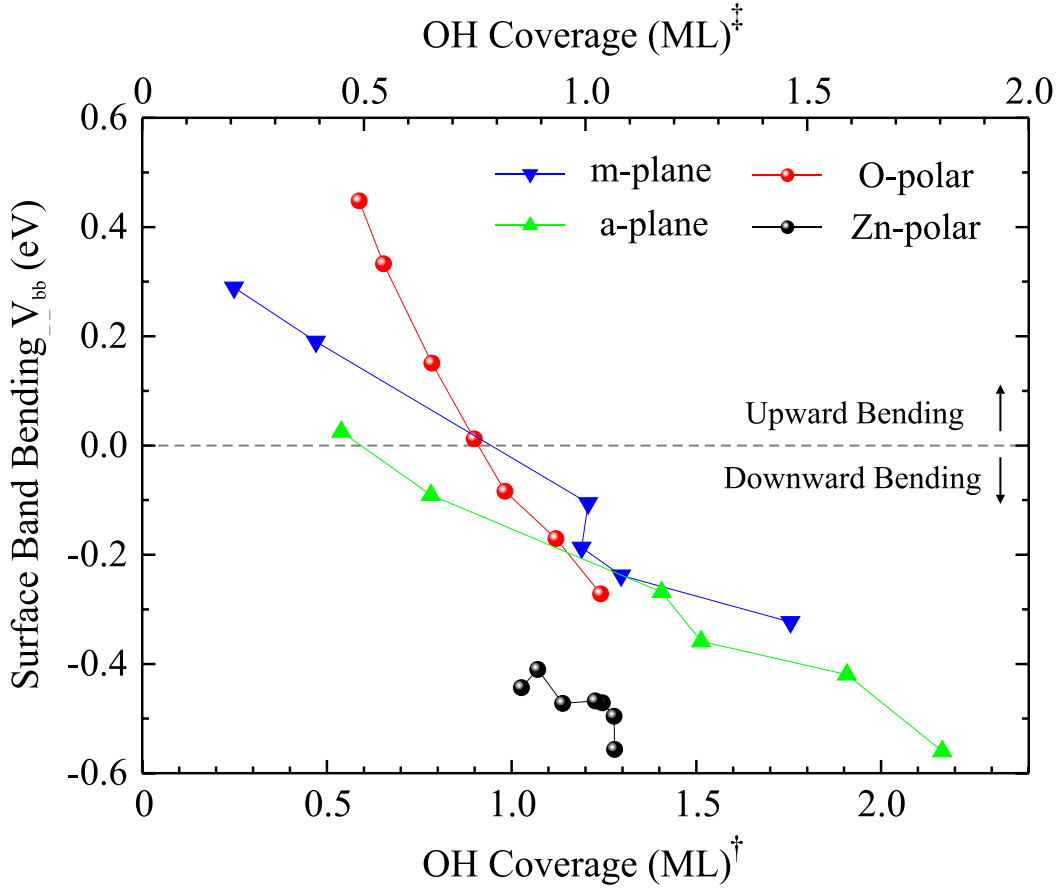
FIG. 6 (Color online) Surface band bending (V_{bb}) versus hydroxyl monolayer coverage on the non-polar m-plane ($10\overline{1}0$) and a-plane ($11\overline{2}0$) faces, and also for the Zn-polar (0001) and O-polar ($000\overline{1}$) faces, of hydrothermal single crystal ZnO extracted via synchrotron XPS following different UHV heat treatments. The horizontal dashed line represents flat near-surface bands. The lower monolayer scale (†) was calculated using a Lambert-Beer approximation, while the upper scale (‡) is based on the physical argument of a closed hydroxyl monolayer on the m-plane ($10\overline{1}0$) face between 200 and 400 ^{o}C, as proposed by Nagao *et al*.[22-24]